An Investigation of Homoclinic Orbits in the Circular Restricted Three-Body Problem

Luke Bury & Don Kuettel

May 2, 2018

Abstract

This paper details the full process for identifying homoclinic orbits in the Circular Restricted Three Body Problem (CR3BP). First, the history of the Henri Poincaré's discovery of homoclinic orbits is briefly discussed. Following this, the CR3BP dynamical system is defined and the process for finding periodic orbits about equilibria in the system is expanded upon. From these periodic orbits, stable and unstable manifolds are determined, and from the intersection of these manifolds, homoclinic orbits are found. Eight homoclinic orbits are identified in the Earth-Moon system.

1 Introduction

In 1885, a competition was held by Acta Mathematica in which participants were challenged to solve one of four outstanding math problems. Henri Poincaré, a prominent mathematician of the time, entered the contest and ultimately won. However, his submission contained a critical mistake that, when corrected, led to the discovery of homoclinic orbits. In mathematics, a homoclinic orbit is defined as a trajectory which joins a saddle equilibrium point to itself. More precisely, a homoclinic orbit is a union between the stable manifold, $W^s(p)$, and the unstable manifold, $W^u(p)$, of an equilibrium point. Figure 1 shows an example of a simple, two-dimensional homoclinic orbit about the saddle equilibrium point p. As the figure shows, as time approaches either negative or positive infinity, the homoclinic orbit will approach p.
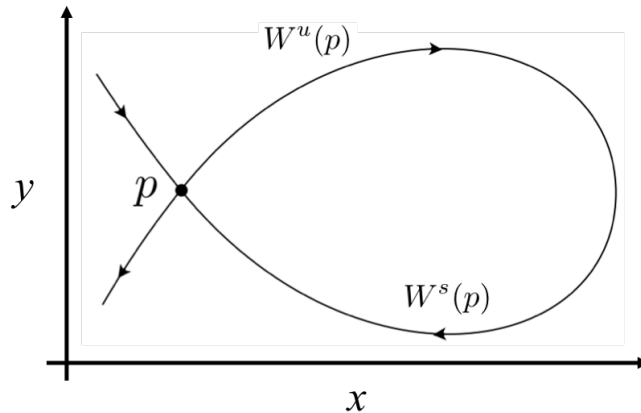

Figure 1: A 2-Dimensional homoclinic orbit.

Homoclinic orbits can reveal much about the chaotic behavior of dynamical systems, but locating these orbits requires a non-trivial, multi-step process. First, a periodic orbit about a

chosen equilibrium point must be identified. From this periodic orbit, both stable and unstable manifolds must be constructed. Finally, intersections of the stable and unstable manifolds are found via Poincaré sections, and homoclinic orbits are thus identified. The following report briefly discusses the history of Poincare's discovery of homoclinic orbits and demonstrates a detailed procedure for locating these orbits. Ultimately, homoclinic orbits in the Earth-Moon system are found and presented.

2 The Competition

As documented by Andersson and Barrow-Green [1, 2], in 1885, Acta Mathematica announced a mathematics competition to the world. This competition, sponsored by King Oscar II of Sweden, encouraged interested parties to make an attempt at solving one of four unanswered problems of the time. Henri Poincaré, a prominant mathematician (who was largely favored to win the competition) attempted the first problem, which essentially asked for a solution to the perplexing n-body problem. Rather than sticking to the exact prompt, Poincaré decided to instead attempt a subset of the n-body problem known as the three-body problem - the first order of the n-body problem remaining unsolved. To further simplify his initial effort, Poincaré restricted the three-body system in a manner known today as the Circular Restricted Three-Body Problem (CR3BP), which will be discussed further in the next section.

Poincaré's submission to the competition was the culmination of several strands of his work from the previous decade, which included geometrical and analytical theory, integral invariants, and periodic solutions to dynamical systems. Poincaré applied these theories in an attempt to rigorously prove stability and find periodic solutions for the CR3BP. The competition judges immediately recognized the importance of Poincaré's submission and unanimously crowned him the victor. However, around the time that his work was first being printed, a discussion with Lars Edvard Phragmén led to the discovery of an error within Poincaré's submission that held significant ramifications. The error was rooted in Poincaré's failing "to take proper account of the exact geometric nature of a particular curve" [3]. In Theorem III of the paper's first, and flawed, edition, Poincaré claimed that a particular invariant curve was closed (Figure 2(a,b)). He failed to consider that the curve could be self-intersecting (Figure 2(c)). After realizing his mistake, Poincaré reworked his derivations to discover that the asymptotic surfaces are not closed, but instead, they intersect along infinitely many asymptotic trajectories. Ironically, this mistake cemented Poincaré's place among legendary mathematicians for his resulting discovery of *doubly asymptotic*, or *homoclinic*, points/orbits in the CR3PB and dynamical systems in general. These curves will resurface in Section 3.5 as the Poincaré sections of intersecting stable and unstable manifolds, where exact intersections of the curves correspond to homoclinic orbits. First, however, the CR3BP and periodic orbits must be well understood.
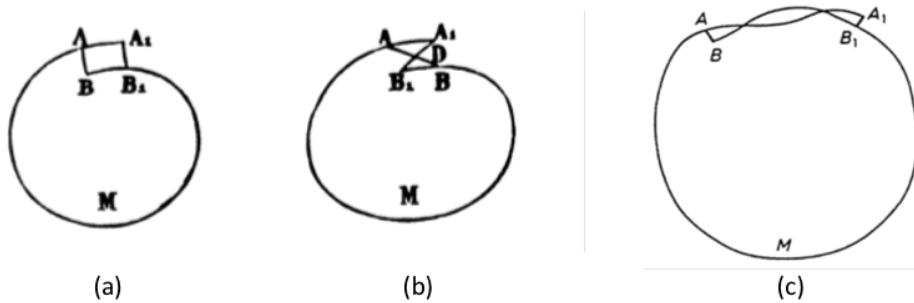

Figure 2: (a) Diagrams of incorrectly closed invariant curves from the first edition of Poincaré's memoir. (b)Invariant curve with self intersection from Poincaré's corrected work [3].

3 Circular Restricted Three Body Problem

Before studying periodic orbits, their manifolds, and the process of locating homoclinic orbits, it is necessary to provide the reader a solid foundation of the Circular Restricted Three Body Problem (CR3BP) - the dynamical system in which the aforementioned trajectories are created and analyzed. In the CR3BP (Fig. 3), the origin of the system is set at the barycenter of the two main bodies in the system (e.g., the Earth & Moon), and the frame rotates so these bodies remain stationary on the x-axis. The bodies are assumed to move in perfectly circular orbits and act as point masses from a gravitational perspective. The restricted problem is then to ascertain the motion of the third body whose mass is considered negligible. The system is normalized in the following ways: the masses of the two primary bodies sum to 1 (i.e., $m_1 = \mu$ and $m_2 = 1 - \mu$, where $\mu = m_2/(m_1 + m_2)$ is known as the three-body parameter); the distance between the primaries is 1; the orbital period period of the primaries is 2π; and the gravitational constant G is equal to 1. Under these conditions, the equations of motion for the CR3BP are shown in Equations 1-3:

$$\ddot{x} = 2\dot{y} + x - (1 - \mu)\left(\frac{x + \mu}{r_1^3}\right) - \mu\left(\frac{x - 1 + \mu}{r_2^3}\right) \tag{1}$$

$$\ddot{y} = -2\dot{x} + y\left(-\frac{1 - \mu}{r_1^3} - \frac{\mu}{r_2^3} + 1\right) \tag{2}$$

$$\ddot{z} = z\left(-\frac{1 - \mu}{r_1^3} - \frac{\mu}{r_2^3}\right), \tag{3}$$

where

$$r_1 = \sqrt{(x + \mu)^2 + y^2 + z^2} \tag{4}$$

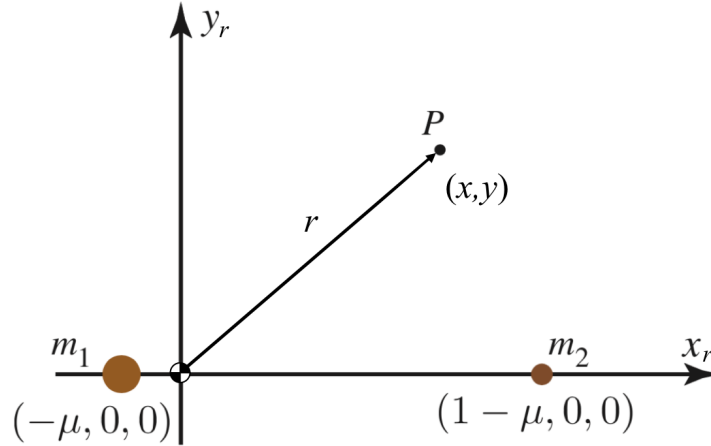$$r_2 = \sqrt{(x - 1 + \mu)^2 + y^2 + z^2}. \tag{5}$$

Figure 3: This figure shows the layout of the Circular Restricted Three-Body Problem [5].

In most simplified astrodynamic systems (e.g., Keplerian motion, CR3BP, n-body porblem, etc...), there are important parameters, known as integrals of motion, that are constant for all motion of a particle in that system. In a Keplerian system, the orbital elements of a trajectory

are the system's integrals of motion. The integral of motion for the CR3PB is called the Jacobi constant and is given by

$$J = -\dot{x}^2 - \dot{y}^2 - \dot{z}^2 + x^2 + y^2 + \frac{2(1-\mu)}{r_1} + \frac{2\mu}{r_2}. \tag{6}$$

For a given Jacobi constant, the motion of a particle is limited to certain regions of space due to the constraint that the velocity cannot have imaginary components. These restrictive regions, whose bounds are known as zero-velocity curves, are computed by setting the velocity in Equation 6 to zero and mapping the resultant contours in the CR3PB. The motion of an object with a specific Jacobi constant is bounded by its respective zero-velocity curve and may only cross the boundaries with the addition of non-conservative force.

3.1 Equilibrium Point Locations

Complex dynamical system such as the CR3PB often times have equilibrium points that result in a constant solution to the system's differential equations. In the CR3BP, these points, known as Lagrange points, are positions where the combined gravitational pull of the two large masses perfectly balances with the centripetal force of the rotating system (i.e., the Lagrange points are stationary within the rotating system of the CR3BP). There are five such points labeled L_1 - L_5 located in the plane of the two primary masses. The first three Lagrange points lie on the line connecting the two primary bodies, and the last two points, L_4 and L_5, are located at the vertex of an equilateral triangle formed with the two primary bodies [5].

In order to find the location of the five equilibrium points in the CR3BP, the velocity and acceleration must be set to zero in the system's equations of motion. This results in the following equations:

$$0 = x - (1-\mu)\left(\frac{x+\mu}{r_1^3}\right) - \mu\left(\frac{x-1+\mu}{r_2^3}\right) \tag{7}$$

$$0 = y\left(-\frac{1-\mu}{r_1^3} - \frac{\mu}{r_2^3} + 1\right) \tag{8}$$

$$0 = z. \tag{9}$$

If y is set to zero, a quintic equation in x emerges. Solving this equation to first order results in the following location for the first three Lagrange points:

$$L_1 = \left(1 - \left(\frac{\mu}{3}\right)^{1/3}, 0, 0\right) \tag{10}$$

$$L_2 = \left(1 + \left(\frac{\mu}{3}\right)^{1/3}, 0, 0\right) \tag{11}$$

$$L_3 = -\left(1 + \left(\frac{5\mu}{12}\right), 0, 0\right). \tag{12}$$

Using Equations 10-12 as initial conditions, a Newton-Raphson iteration can then be used to numerically find the location of the first three Lagrange points to machine precision. Equations 7-9 can also be used to find the two triangular equilibrium points, L_4 and L_5. Since these equilibrium points form an equilateral triangle with the primary bodies [5], $r_1 = r_2 = 1$ is substituted into Equation 7 and Equation 8. These equations are subsequently solved to provide the exact locations for the remaining equilibrium points:

4

$$L_4 = \left(\frac{1}{2} - \mu, \frac{\sqrt{3}}{2}, 0 \right) \tag{13}$$

$$L_5 = \left(\frac{1}{2} - \mu, -\frac{\sqrt{3}}{2}, 0 \right). \tag{14}$$

Using the Earth-Moon CR3BP three-body parameter ($\mu = 0.012155$), Table 1 shows the non-dimensional locations of the five Lagrange points to six significant digits. Additionally, Figure 4 graphically shows these locations along with a contour plot of the Earth-Moon CR3BP's zero-velocity curves for varying Jacobi constants. As Figure 4 shows, L_1, L_2, and L_3 lie at saddle points, while L_4 and L_5 lie at extrema values.

Table 1: Summary of the Dimensionless Earth-Moon CR3BP Equilibrium Points

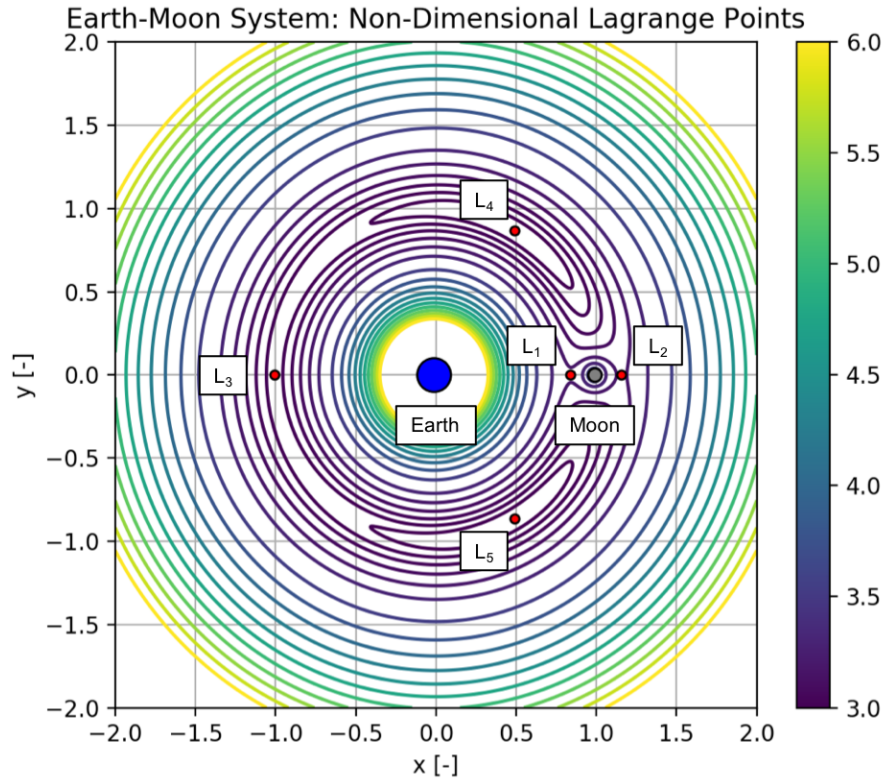| Lagrange Point	x	y	z
L_1	0.836893	0	0
L_2	1.15570	0	0
L_3	-1.00506	0	0
L_4	0.487845	0.866025	0
L_5	0.487845	-0.866025	0

Figure 4: This figure depicts the the 5 equilibrium points and the zero-velocity curves in the non-dimensional Earth-Moon CR3BP system.

3.2 Equilibrium Point Stability

In this section, a planar stability analysis is performed about each Lagrange point in the Earth-Moon CR3BP. This study entails linearizing the CR3BP equations of motion about each equilibrium point and solving for the eigenvalues at that point. The CR3BP equations of motion can be linearized by taking a Taylor series expansion of the ODE about each equilibrium point in the system. Neglecting higher order terms, the linearized equations of motion are given by

$$
\delta \begin{bmatrix} \dot{x} \\ \dot{y} \\ \ddot{x} \\ \ddot{y} \end{bmatrix} = Df\left(x^*, y^*, \dot{x}^*, \dot{y}^*\right) \begin{bmatrix} x \\ y \\ \dot{x} \\ \dot{y} \end{bmatrix},
\tag{15}
$$

where

$$
Df\left(x, y, \dot{x}, \dot{y}\right) = \begin{bmatrix}
\frac{\partial \dot{x}}{\partial x} & \frac{\partial \dot{x}}{\partial y} & \frac{\partial \dot{x}}{\partial \dot{x}} & \frac{\partial \dot{x}}{\partial \dot{y}} \\
\frac{\partial \dot{y}}{\partial x} & \frac{\partial \dot{y}}{\partial y} & \frac{\partial \dot{y}}{\partial \dot{x}} & \frac{\partial \dot{y}}{\partial \dot{y}} \\
\frac{\partial \ddot{x}}{\partial x} & \frac{\partial \ddot{x}}{\partial y} & \frac{\partial \ddot{x}}{\partial \dot{x}} & \frac{\partial \ddot{x}}{\partial \dot{y}} \\
\frac{\partial \ddot{y}}{\partial x} & \frac{\partial \ddot{y}}{\partial y} & \frac{\partial \ddot{y}}{\partial \dot{x}} & \frac{\partial \ddot{y}}{\partial \dot{y}}
\end{bmatrix}.
\tag{16}
$$

For the CR3BP, Equation 16 evaluates to

$$
Df\left(x, y, \dot{x}, \dot{y}\right) = \begin{bmatrix}
0 & 0 & 1 & 0 \\
0 & 0 & 0 & 1 \\
XX & XY & 0 & 2 \\
YX & YY & -2 & 0
\end{bmatrix},
\tag{17}
$$

where

$$
XX = \frac{\mu - 1}{r_1^3} - \frac{\mu}{r_2^3} + \frac{3\mu\left(\mu + x - 1\right)^2}{r_2^5} - \frac{3\left(\mu + x\right)^2\left(\mu - 1\right)}{r_1^5} + 1
\tag{18}
$$

$$
XY = YX = \frac{3\mu y\left(\mu + x - 1\right)}{r_2^5} - \frac{3y\left(\mu + x\right)\left(\mu - 1\right)}{r_1^5}
\tag{19}
$$

$$
YY = \frac{\mu - 1}{r_1^3} - \frac{\mu}{r_2^3} + \frac{3\mu y^2}{r_2^5} - \frac{3y^2\left(\mu - 1\right)}{r_1^5} + 1.
\tag{20}
$$

By evaluating the Jacobian given in Equation 17 at each equilibrium point and finding the resulting eigenvalues, the stability of these points can be ascertained.

3.2.1 L$_1$, L$_2$, and L$_3$ Stability

It was shown in Figure 4 that L$_1$, L$_2$, and L$_3$ are saddle points. By plugging in the locations of the equilibrium points given in Table 1 along with the Earth-Moon three-body parameter ($\mu = 0.012155$), this claim can be mathematically validated.

L₁

The evaluated Df matrix for the L$_1$ Lagrange point is given by

$$Df|_{L_1} = \begin{bmatrix} 0 & 0 & 1 & 0 \\ 0 & 0 & 0 & 1 \\ 11.2955 & 0 & 0 & 2 \\ 0 & -4.1478 & -2 & 0 \end{bmatrix}, \tag{21}$$

where

$$\lambda_{1,2} = \pm 2.9321 \text{ and } \lambda_{3,4} = \pm i2.3344. \tag{22}$$

As Equation 22 shows, the L$_1$ equilibrium point has a positive/negative real eigenvalue pair that results in a dynamically unstable saddle point. Small departures from the equilibrium will grow exponentially with a time constant of $\tau = 1/real(\lambda_{3,4}) = 0.4284$. Re-dimensionalizing this value by the rotation rate of the Earth-Moon system ($\omega = 2.665 \times 10^{-6}$ rad/sec) results in a time constant of $\tau \approx 1.86$ days. In other words, a satellite parked at L$_1$ will wander off after a few days unless course corrections are made.

L₂

The evaluated Df matrix for the L$_2$ Lagrange point is given by

$$Df|_{L_2} = \begin{bmatrix} 0 & 0 & 1 & 0 \\ 0 & 0 & 0 & 1 \\ 7.3807 & 0 & 0 & 2 \\ 0 & -2.1903 & -2 & 0 \end{bmatrix}, \tag{23}$$

where

$$\lambda_{1,2} = \pm 2.1586 \text{ and } \lambda_{3,4} = \pm i1.8626. \tag{24}$$

Similarly to the L$_1$ point, the L$_2$ Lagrange point has a positive/negative real eigenvalue pair that results in a dynamically unstable saddle point. The re-dimensionalized L$_2$ time constant is $\tau \approx 2.33$ days.

L₃

The evaluated Df matrix for the L$_3$ Lagrange point is given by

$$Df|_{L_3} = \begin{bmatrix} 0 & 0 & 1 & 0 \\ 0 & 0 & 0 & 1 \\ 3.0214 & 0 & 0 & 2 \\ 0 & -0.0107 & -2 & 0 \end{bmatrix}, \tag{25}$$

where

$$\lambda_{1,2} = \pm0.1779 \text{ and } \lambda_{3,4} = \pm i1.0104. \tag{26}$$

Once again, the evaluated Df matrix has a positive/negative real eigenvalue pair resulting in the L$_3$ Lagrange point being an unstable saddle point. The re-dimensionalized L$_3$ time constant is $\tau \approx 4.30$ days.

3.2.2 L$_4$ and L$_5$ Stability

The stability analysis of the L$_4$ and L$_5$ Lagrange points yields a surprise. While these points correspond to local maxima of the total potential, they are stable due to a "Coriolis" force. To prove this, the evaluated Df matrix for the L$_4$ and L$_5$ Lagrange points is given by

$$Df|_{L_4,5} = \begin{bmatrix} 0 & 0 & 1 & 0 \\ 0 & 0 & 0 & 1 \\ 0.7500 & \pm1.2675 & 0 & 2 \\ \pm1.2675 & 2.2500 & -2 & 0 \end{bmatrix}, \tag{27}$$

where

$$\lambda_{1,2} = \pm i0.9545 \text{ and } \lambda_{3,4} = \pm i0.2983. \tag{28}$$

As Equation 28 shows, the L$_4$ and L$_5$ equilibrium points have purely imaginary eigenvalues in the Earth-Moon system resulting in Lyapunov stability. However, this is not always the case for a three body system. In order for the L$_4$ and L$_5$ Lagrange points to be stable, the primary masses of the system have to satisfy the following inequality [8]

$$\frac{m_1}{m_2} > \frac{25 + \sqrt{621}}{2} \approx 24.96. \tag{29}$$

For reference, $m_1/m_2 = 81.27$ for the Earth-Moon system. Now that the Earth-Moon equilibrium points have been identified, numerical methods can be used to generate families of periodic orbits about these points.

3.3 Periodic Orbits

The solution flow of a dynamical system is often times denoted $\boldsymbol{x}(t) = \boldsymbol{\varphi}(t;\boldsymbol{x}_0)$ with initial condition $\boldsymbol{x}(t_0) = \boldsymbol{\varphi}(t_0;\boldsymbol{x}_0)$. A periodic orbit is a solution of the system such that $\boldsymbol{\varphi}(t+T;\boldsymbol{x}_0) = \boldsymbol{\varphi}(t;\boldsymbol{x}_0)$ for all t where $T > 0$ is the period of the orbit. Lyapunov's Center Theorem states that for a system with an integral of motion (the Jacobi constant in the case of the CR3BP), if $Df(\boldsymbol{x}^*)$ has eigenvalues $\pm i\omega, \lambda_3, \lambda_4, ..., \lambda_n$ (i.e., at least one center manifold), then there exists a one-parameter family of periodic orbits emanating from the equilibrium point. Furthermore, periods tend toward $2\pi/\omega$ when approaching the equilibrium point along the family [6]. Using this knowledge, one of the most straightforward methods used to solve for periodic orbit families is to make educated guesses at individual periodic orbit initial conditions and then use a single shooter algorithm to correct them.

3.3.1 Family Finding Algorithm

The family finding algorithm (FFA) begins by determining the dynamical system's fundamental matrix $\Phi(t, t_0)$. In a system as complicated as the CR3BP, Φ must be computed numerically

through the following differential equation

$$\dot{\Phi} = Df\left(\boldsymbol{x}\right)\Phi \text{ with } \Phi\left(t_0, t_0\right) = \mathcal{I}. \tag{30}$$

The full dynamics matrix Df, which was touched on in Equation 17, is given by

$$Df = \begin{bmatrix} 0_{3\times 3} & \mathcal{I}_{3\times 3} \\ \Omega_{i,j} & V \end{bmatrix} \tag{31}$$

where $\mathcal{I}$ is a 3×3 identity matrix, V is given by

$$V = \begin{bmatrix} 0 & 2 & 0 \\ -2 & 0 & 0 \\ 0 & 0 & 0 \end{bmatrix}, \tag{32}$$

and $\Omega_{i,j}$ is a 3×3 matrix of second order partial derivatives $(\Omega_{i,j} = \Omega_{j,i})$ given by

$$\Omega_{x,x} = \frac{\partial\ddot{x}}{\partial x} = \frac{\mu - 1}{r_1^3} - \frac{\mu}{r_2^3} + \frac{3\mu\left(\mu + x - 1\right)^2}{r_2^5} - \frac{3\left(\mu + x\right)^2\left(\mu - 1\right)}{r_1^5} + 1 \tag{33}$$

$$\Omega_{y,y} = \frac{\partial\ddot{y}}{\partial y} = \frac{\mu - 1}{r_1^3} - \frac{\mu}{r_2^3} + \frac{3\mu y^2}{r_2^5} - \frac{3y^2\left(\mu - 1\right)}{r_1^5} + 1 \tag{34}$$

$$\Omega_{z,z} = \frac{\partial\ddot{z}}{\partial z} = \frac{\mu - 1}{r_1^3} - \frac{\mu}{r_2^3} + \frac{3\mu z^2}{r_2^5} - \frac{3z^2\left(\mu - 1\right)}{r_1^5} \tag{35}$$

$$\Omega_{x,y} = \frac{\partial\ddot{x}}{\partial y} = \frac{3\mu y\left(\mu + x - 1\right)}{r_2^5} - \frac{3y\left(\mu + x\right)\left(\mu - 1\right)}{r_1^5} \tag{36}$$

$$\Omega_{y,z} = \frac{\partial\ddot{y}}{\partial z} = \frac{3\mu z\left(\mu + x - 1\right)}{r_2^5} - \frac{3z\left(\mu + x\right)\left(\mu - 1\right)}{r_1^5} \tag{37}$$

$$\Omega_{z,x} = \frac{\partial\ddot{z}}{\partial x} = \frac{3\mu yz}{r_2^5} - \frac{3yz\left(\mu - 1\right)}{r_1^5}. \tag{38}$$

Using the aforementioned Lyapunov Center Theorem, the FFA is initiated by perturbing the equilibrium point of interest in the direction of a center manifold (purely imaginary eigenvalue) by a small amount ($\epsilon < 1 \times 10^{-4}$). This results in the "smallest" periodic orbit around the equilibrium point. The period of the orbit is then determined by the value of the eigenvalue ($T = 2\pi/\lambda$). To continue the FFA, future periodic orbit initial conditions ($\boldsymbol{x}_0, T$) are calculated by adding small perturbations to the previous periodic orbit initial conditions ($\tilde{\boldsymbol{x}}_0, \tilde{T}$) in the orbit tangent direction ($\tilde{\boldsymbol{x}}_0', \tilde{T}'$). This update is mathematically shown as:

$$\boldsymbol{x}_0 = \tilde{\boldsymbol{x}}_0 + \Delta s\tilde{\boldsymbol{x}}_0' \tag{39}$$
$$T = \tilde{T} + \Delta s\tilde{T}', \tag{40}$$

where Δs is the step size between the original periodic orbit and the new periodic orbit and the orbit tangent direction is approximated by the change in the initial conditions between two previous orbits. In order to ensure that the new periodic orbit is part of the periodic orbit family, two important constraints must be satisfied. The first constraint, known as the Poincaré phase condition, which assumes that a periodic orbit in the family has already been computed, states that

$$< \boldsymbol{x}_0 - \tilde{\boldsymbol{x}}_0, \boldsymbol{f}\left(\tilde{\boldsymbol{x}}_0\right) >= 0, \tag{41}$$

where $\boldsymbol{f}(\boldsymbol{x})$ are the dynamics of the CR3BP evaluated at some state. The second constraint, known as the pseudo-arclength continuation constraint, which assumes that a periodic orbit in the family and an approximation of the tangent to the solution family has already been computed, states that

$$< \boldsymbol{x}_0 - \tilde{\boldsymbol{x}}_0, \tilde{\boldsymbol{x}}_0' > + \left(T - \tilde{T}\right)\tilde{T}' = \Delta s. \tag{42}$$

Using these constraints, a system of equations for the FFA is given by

$$\begin{bmatrix} \varphi\left(T;\boldsymbol{x}_0\right) - \boldsymbol{x}_0 \\ < \boldsymbol{x}_0 - \tilde{\boldsymbol{x}}_0, \boldsymbol{f}\left(\tilde{\boldsymbol{x}}_0\right) > \\ < \boldsymbol{x}_0 - \tilde{\boldsymbol{x}}_0, \tilde{\boldsymbol{x}}_0' > + \left(T - \tilde{T}\right)\tilde{T}' - \Delta s \end{bmatrix} = \boldsymbol{F}\left(\boldsymbol{x}_0, T\right) = \boldsymbol{0}, \tag{43}$$

where $\boldsymbol{x}_0$ and T are unknowns. This system of equations is then solved using a single shooter algorithm [7] which is given in the form

$$\begin{bmatrix} \Phi\left(T\right) - \mathcal{I}_{n \times n} & \boldsymbol{f}\left(\boldsymbol{x}\left(T\right)\right) \\ \dot{\tilde{\boldsymbol{x}}}_0 & 0 \\ \tilde{\boldsymbol{x}}_0' & \tilde{T}' \end{bmatrix} \begin{bmatrix} \delta\boldsymbol{x}_0 \\ \delta T \end{bmatrix} = -\boldsymbol{F}\left(\boldsymbol{x}_0, T\right), \tag{44}$$

where $\delta\boldsymbol{x}_0$ and δT are updates to the initial conditions of the new periodic orbit. Since the single shooter algorithm uses a first-order Newton-Raphson method, Equation 44 is iterated until convergence. Furthermore, since this system is overdetermined ($n+2$ equations and $n+1$ unknowns), a pseudo-inverse is used when solving for $\delta\boldsymbol{x}_0$ and δT. An example of the single shooter algorithm correcting a periodic orbit is shown in Figure 5. Using this FFA, a periodic orbit family can be calculated with minimal a priori knowledge for as many number of periodic orbits as desired.
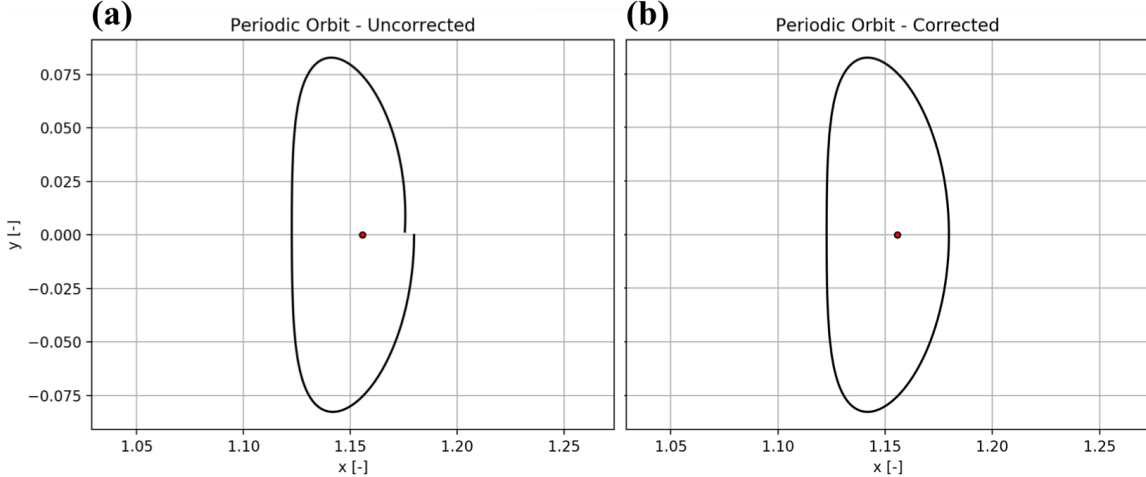

Figure 5: This figure shows the single shooter algorithm correcting a periodic orbit. Figure (a) shows the uncorrected orbit, and Figure (b) shows the correct orbit.

3.3.2 Orbit Families

In 1892, Poincaré showed that an infinite number of periodic solutions exist in the three-body problem [2]. These solutions come in a variety of forms that include planar Lypaunov periodic orbits, 3-dimensional clamshell orbits, 3-dimensional halo orbits, and many others. All of these periodic orbit solutions intersect and merge with one another through complex interactions and bifurcations. Using the previously described FFA, all of these periodic orbit families can be cataloged. Figure 4 shows an example of planar Lypaunov periodic orbit families calculated about each of the five Lagrange points. Additionally, Figure 7 shows 3-dimensional clamshell orbits about L_1.
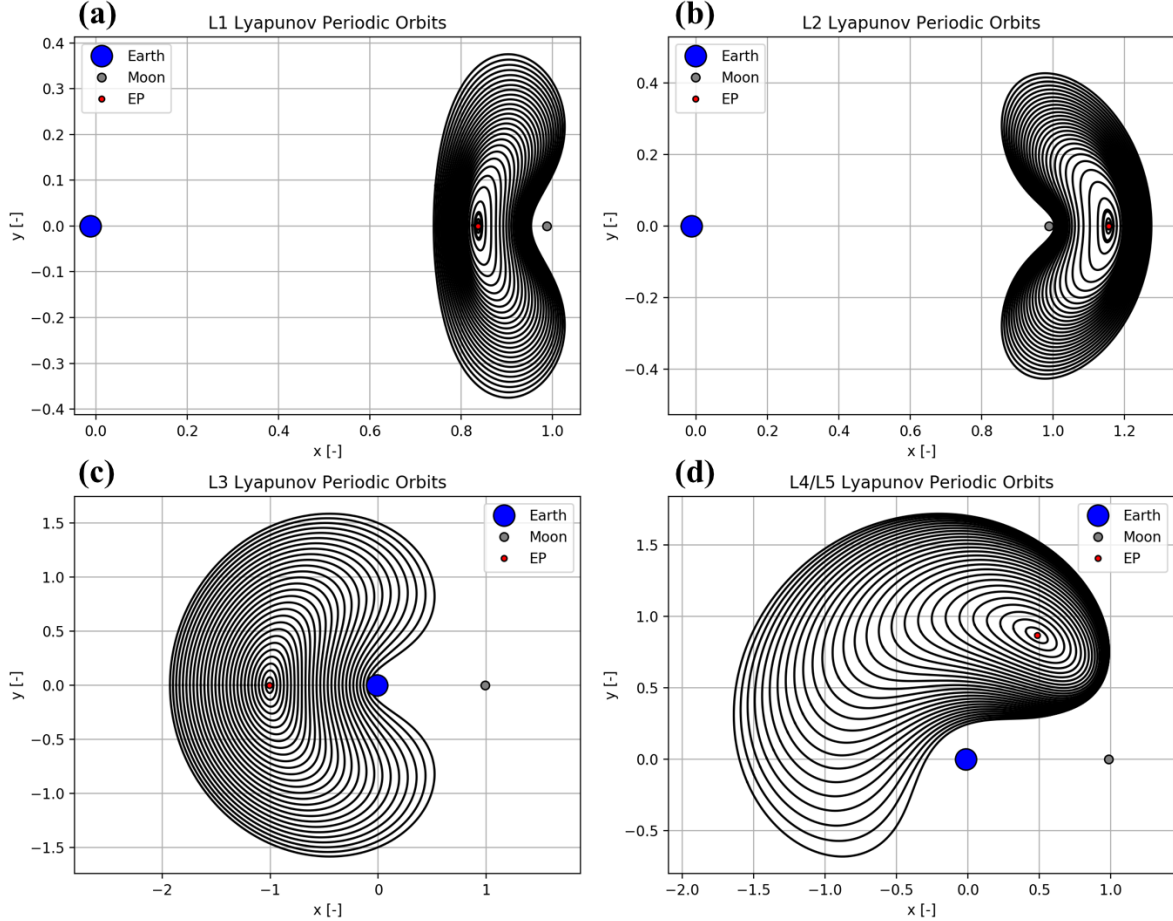

Figure 6: This figure shows planar Lypaunov periodic orbit families about each of the five Lagrange points. Figure (a) shows orbits about L_1, Figure (b) shows orbits about L_2, Figure (c) shows orbits about L_3, Figure (d) shows orbits about $L_{4,5}$.
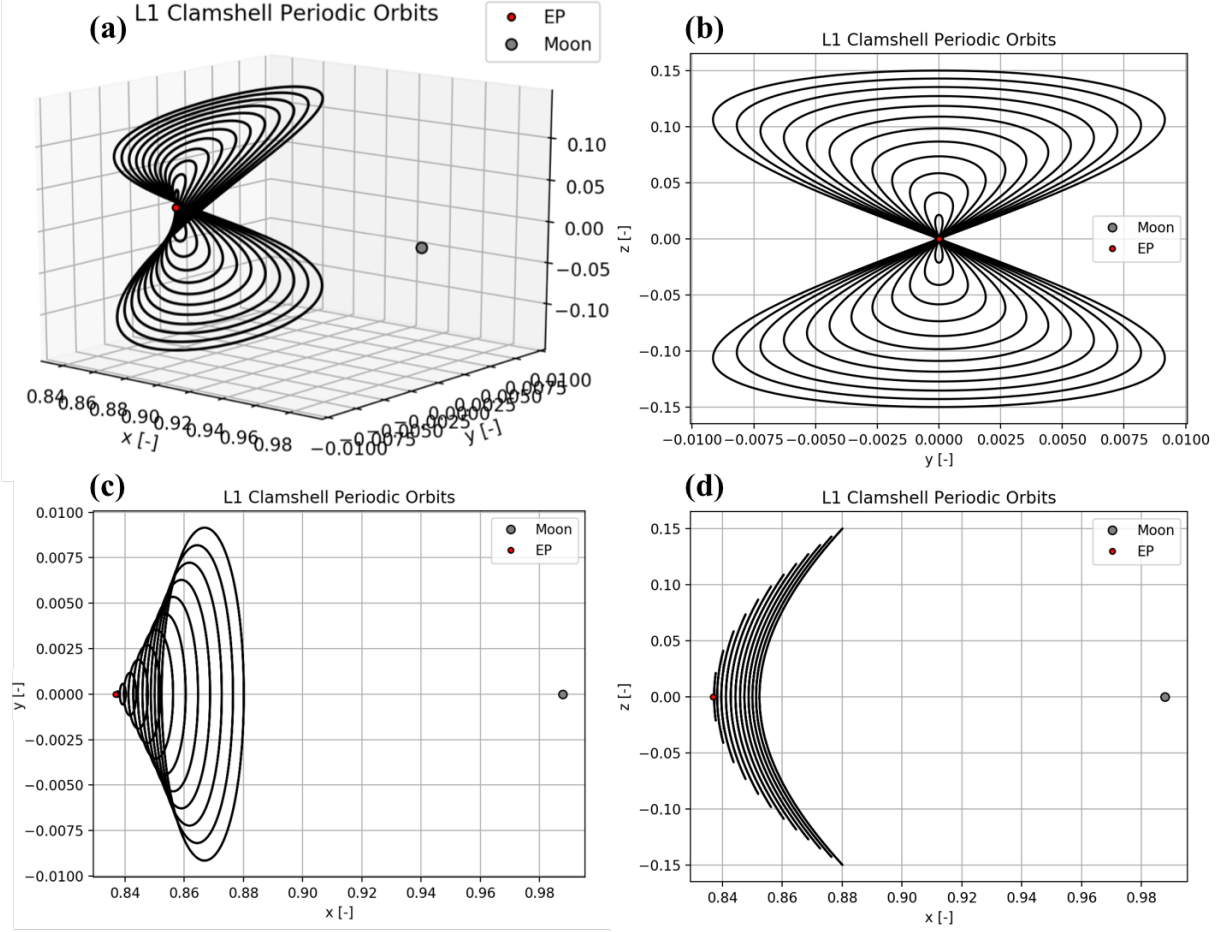
Figure 7: This figure shows a family of 3-dimensional clamshell orbits about L_1.

3.4 Periodic Orbit Stability and Manifolds

In dynamical systems, periodic orbits are invariant sets (i.e., for each $x \in \Lambda, \varphi(t; x) \in \Lambda$ for any t), and as such, their stability can be discussed. In order to determine the stability of a periodic orbit, the eigenvalues of the orbit's Monodromy matrix, which is defined as a periodic orbit's fundamental matrix evaluated after one period T (i.e., $M = \Phi(t_0 + T, t_0)$), need to be analyzed. For the CR3BP, the Monodromy matrix has six eigenvalues and six corresponding eigenvectors. Since M is symplectic, the eigenvalues will come in 3 pairs with one of the pairs always being equal to 1. The relationship between the eigenvalues is as follows

$$\lambda_1 = \frac{1}{\lambda_2} \tag{45}$$

$$\lambda_3 = \frac{1}{\lambda_4} \tag{46}$$

$$\lambda_5 = \lambda_6 = 1. \tag{47}$$

The eigenvalues of the Monodromy matrix reveal the effects of small perturbations on periodic orbits. If the real components of the eigenvalue are between -1 and 1, a perturbation in that direction will exponentially decay and the orbit is considered stable. This is due to the fact that the eigenvalues of the Monodromy M are related to the eigenvalues of the Jacobian matrix Df as $(\lambda_i, 1/\lambda_i) = (e^{\sigma t}, e^{-\sigma t})$, where σ is the eigenvalue of Df. Conversely, if the real com-

ponents are outside of -1 and 1, a perturbation in that direction will exponentially grow and the orbit is considered unstable. If the eigenvalue is only imaginary, then the perturbation will oscillate about the original state after each period. Finally, if the eigenvalues are equal to 1, the perturbation does not grow or decay (unit eigenvalues are therefore normally ignored).

In order to map a stable or unstable manifold of a periodic orbit, the initial conditions of the orbit must be perturbed in the direction of the manifold (i.e., in the direction of the eigenvector corresponding to the manifold of interest). To fully map these manifolds, the periodic orbit needs to be perturbed at many points along its trajectory. This is accomplished by using the fundamental matrix to map the original stable or unstable eigenvector $\boldsymbol{v}^{S,U}$ from M to any point on the periodic orbit (i.e., $\boldsymbol{v}_i^{S,U} = \Phi\left(t_i, t_0\right) \boldsymbol{v}^{S,U}$). The periodic orbit is then perturbed by a small amount ($\epsilon < 1 \times 10^{-4}$) in the direction of the mapped eigenvector (i.e., $\boldsymbol{x}_i^{S,U} = \boldsymbol{x}_i \pm \epsilon|\boldsymbol{v}_i^{S,U}|$). To see the shape of each manifold, the unstable manifold is then propagated forward in time while the stable manifold is propagated backwards in time. Each periodic orbit in the CR3BP has both interior and exterior stable and unstable manifolds depending on the sign of the applied perturbation. Figure 8 shows the exterior stable (green) and unstable (red) manifolds of a L_2 Lyapunov periodic orbit. As Figure 8 shows, these manifolds are intricate structures that extend far into the CR3BP phase space.
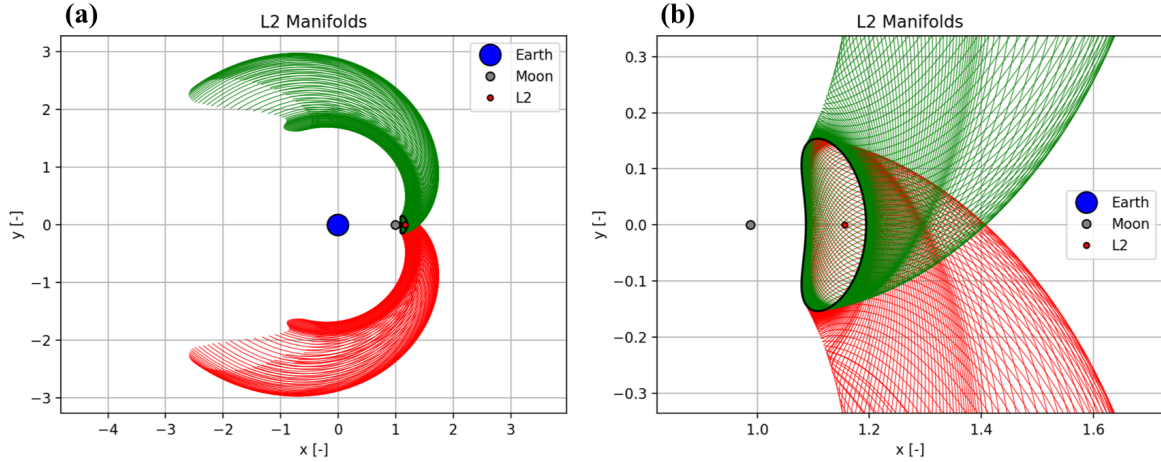

Figure 8: This figure shows the exterior stable (green) and unstable (Red) manifolds of a L_2 Lyapunov periodic orbit.

3.5 Poincaré Sections and Homoclinic Orbits

In a dynamical system, an orbit Γ is homoclinic if each $x \in \Gamma$ is both forward and backwards asymptotic to the same invariant set Λ. In other words, for any $x \in \Gamma$ as $t \to \pm\infty$, $x \to \Lambda$. In order for this to occur, a homoclinic orbit must be contained in the intersection of the stable $W^S\left(\Lambda\right)$ and unstable $W^U\left(\Lambda\right)$ manifolds of the invariant set (i.e., $\Gamma \subset W^S\left(\Lambda\right) \cap W^U\left(\Lambda\right)$). Classically, a mathematical technique known as a Poincaré section is used to find the intersection of $W^S\left(\Lambda\right)$ and $W^U\left(\Lambda\right)$.

In the CR3BP, a Poincaré section, which is defined as lower dimensional surface of section that is transverse to the flow of a dynamical system, is used to map the characteristics of the stable ($W^S\left(\Lambda\right)$) and unstable ($W^U\left(\Lambda\right)$) manifolds of a periodic orbit (Λ). Figure 9 shows an example of a Poincaré section for two different periodic orbits about the L_2 Lagrange point. In the CR3BP, a common Poincaré section for the L_2 Lagrange point is the surface $y = 0$ and $x < 0$. This surface is indicated in Figure 9a and Figure 9b as the thick black line at $y = 0$. In order to find the intersection of the stable (green) and unstable (red) manifolds of the periodic orbit, both manifolds are propagated (as described in the previous section) to the Poincaré section where

their x-position and x-velocity are recorded. The position and velocity of both manifolds are then plotted against one another, as shown in Figure 9c and Figure 9d, to determine if there is any intersection points between the two manifolds (i.e., $\Gamma \subset W^S(\Lambda) \cap W^U(\Lambda)$). In other words, the intersections of the stable and unstable manifolds on the Poincaré section represent a state shared by both manifolds, thus a state belonging to a homoclinic orbit. A careful inspection of Figure 9d reveals that there are eight intersection points in between $W^S(\Lambda)$ and $W^U(\Lambda)$ corresponding to eight different homoclinic orbits for the periodic orbit in question. However, it is important to note that not every periodic orbit has homoclinic trajectories, as Figure 9c shows.
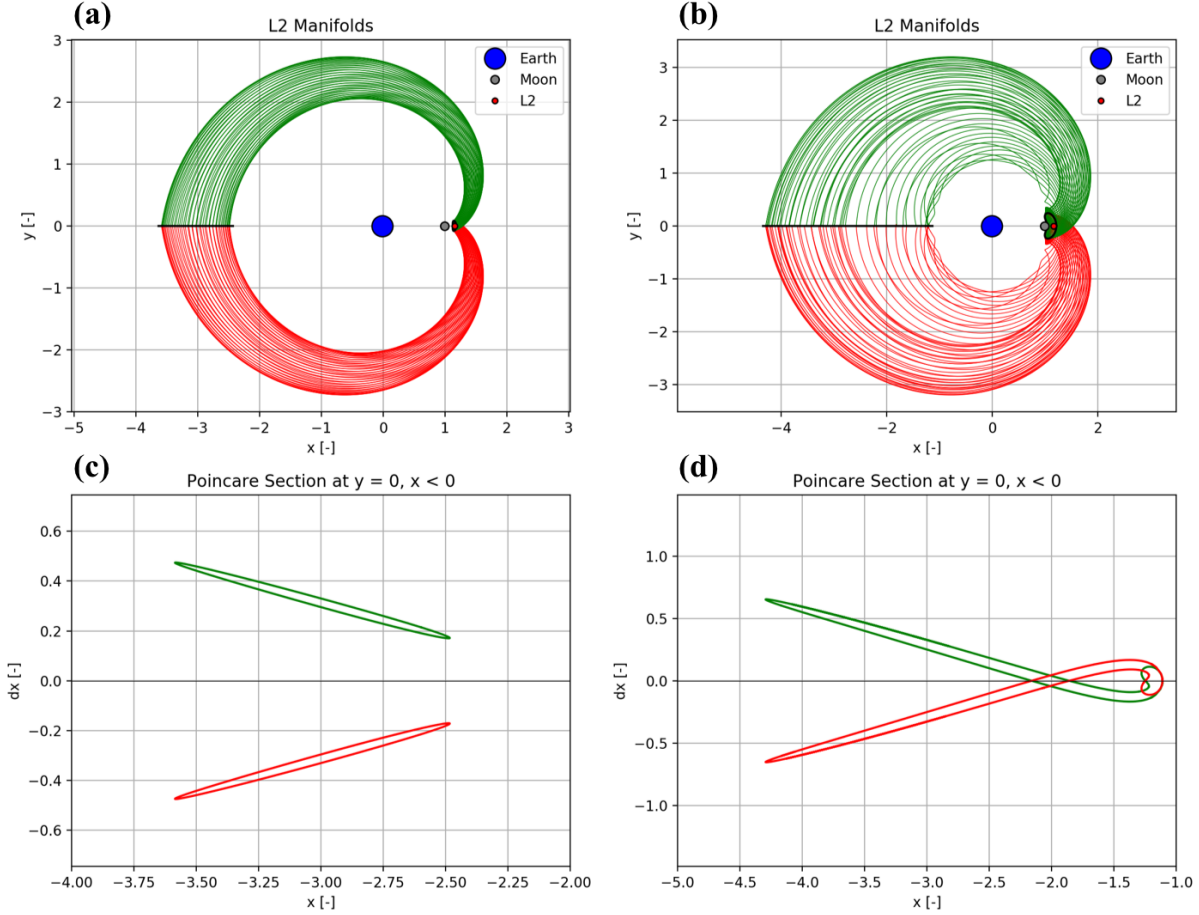

Figure 9: This figure shows the construction of a Poincaré section for two different periodic orbits about the L$_2$ Lagrange point.

Figure 10a takes a closer look at the intersection of the stable and unstable manifolds of the periodic orbit shown in Figure 9b. As Figure 10a shows, there are four intersection points located on the line $\dot{x} = 0$ and four points located off of line $\dot{x} = 0$. The manifold intersection points that lie on the line $\dot{x} = 0$ represent symmetric homoclinic orbits, whereas the points that lie off the line represent asymmetric homoclinic orbits. An example of these different types of orbits can be seen in Figure 10b and Figure 11b, respectively. As Figure 10b and Figure 11b show, the two homoclinic orbits depart from the periodic orbit on the unstable manifold (red) and return to the periodic orbit on the stable manifold (green). Finding the exact initial conditions for homoclinic orbits is computationally taxing due to their extreme sensitivity in the CR3BP.
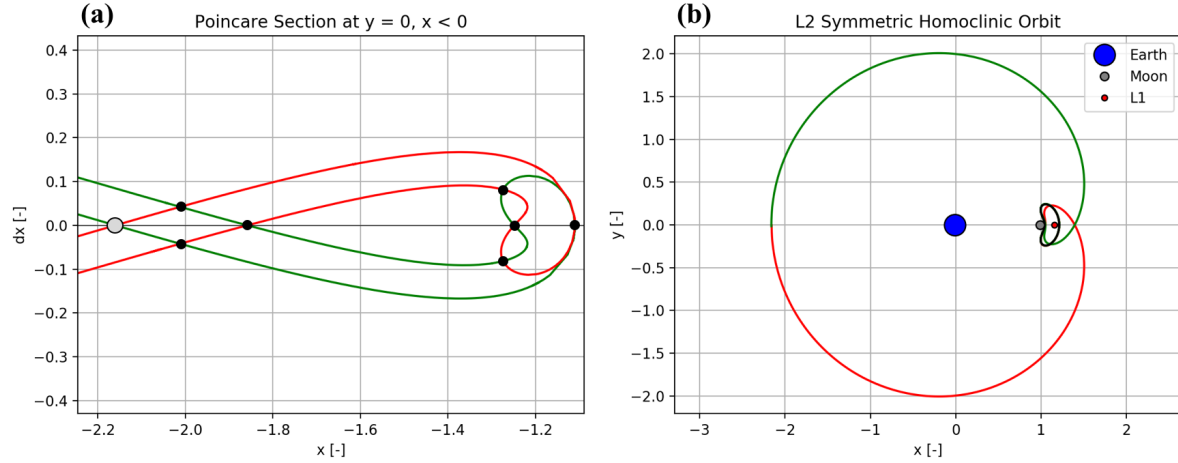
Figure 10: This figure shows a symmetric homoclinic orbit about the L_2 Lagrange point. The grey dot in Figure (a) represents the homoclinic orbit investigated.
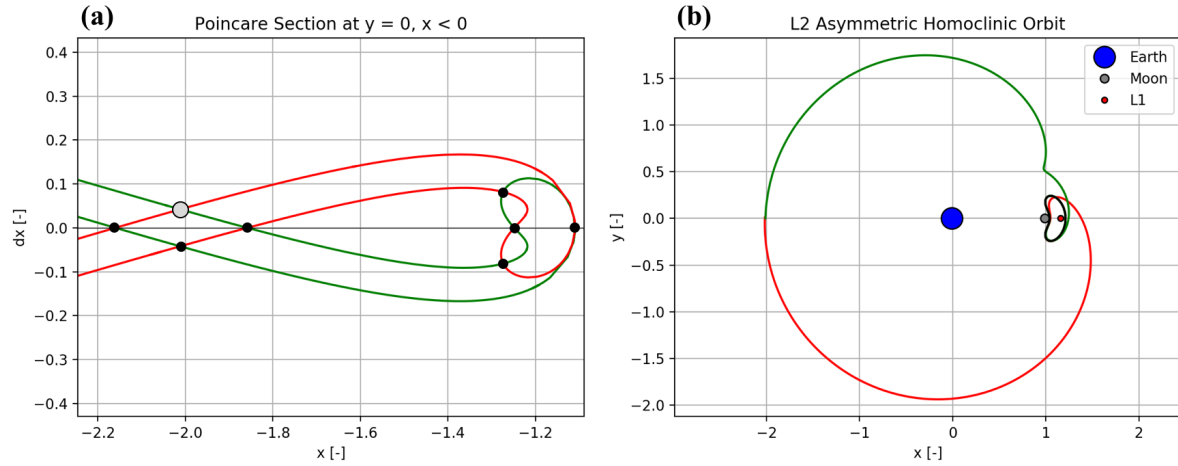

Figure 11: This figure shows a asymmetric homoclinic orbit about the L_2 Lagrange point. The grey dot in Figure (a) represents the homoclinic orbit investigated.

4 Conclusion

Although the process of identifying homoclinic orbits is highly involved and computationally expensive, it exposes much about the intricacies of these dynamical systems. For example, in mission design, a complete understanding of periodic orbits is very helpful for designing trajectories with repeating ground-tracks that may be ideal for scientific investigation. Furthermore, the stable and unstable manifolds of these periodic orbits can be used to target periodic orbits from far away and for transporting a spacecraft around a system for very little fuel costs. Figure 12a makes this clear by illustrating both the interior and exterior manifolds of L_1 and L_2 periodic orbits. In the figure, trajectories connecting the manifolds at U_1 and U_4 are homoclinic orbits. On the contrary, the manifolds shown at U_2 and U_3 originate from different periodic orbits. Trajectories connecting these manifolds are known as heteroclinic orbits. In addition to allowing a spacecraft to traverse a single three-body system, heteroclinic orbits from stable

and unstable manifolds from different three-body systems can be patched together to create a strategy for exploring multi-body systems with minimal fuel use, as shown in Figure 12b.

Henri Poincaré was ashamed for making such a critical mistake in his award-winning submission to Acta Mathematica, but in doing so he discovered homoclinic orbits and greatly expanded the field of dynamical systems. More than 130 years later, his discovery is still being studied and helping humanity to explore the mysteries of space. We'll never forget you, Henri.
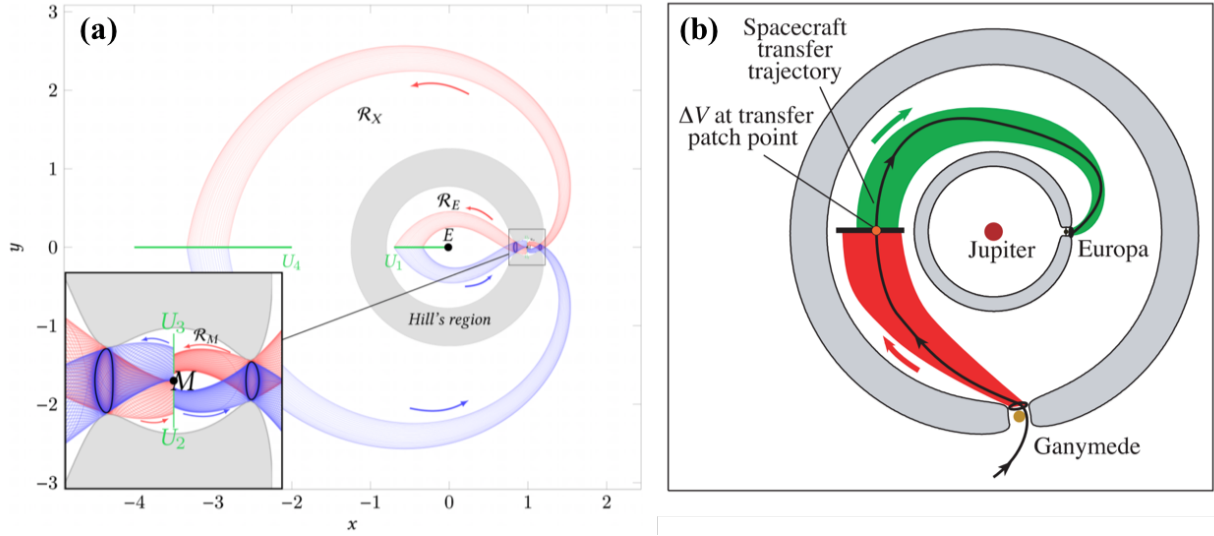

Figure 12: Figure (a) depicts a full mapping of the interior and exterior, stable and unstable, L_1 and L_2 Lagrange points to appropriate Poincaré sections [5]. Figure (b) demonstrates that stable and unstable manifolds can be used to design tours of multi-body systems by riding the unstable manifold of one 3-body system to the stable manifold of another [4].

References

[1] K. G. Andersson. Poincaré's discovery of homoclinic points. *Archive for History of Exact Sciences*, 48(2):133–147, 1994.

[2] J. Barrow-Green. Oscar ii's prize competition and the error in poincaré's memoir on the three body problem. *Archive for History of Exact Sciences*, 48(2):107–131, 1994.

[3] J. Barrow-Green. *Poincaré and the Three Body Problem.* American Mathematical Society, 1997.

[4] G. Gomez, W. S. Koon, M. W. Lo, J. E., Marsden, and S. D. Ross. Connecting orbits and invariant manifolds in the spatial restricted three-body problem. *Institute of Physics Publishing - Nonlinearity*, 17:1571–1606, 2004.

[5] W. S. Koon, M. W. Lo, J. E., Marsden, and S. D. Ross. *Dynamical Systems, The Three-Body Problem, and Space Mission Design.* Marsden Books, 2011.

[6] Kenneth Meyer, Glen Hall, and Dan Offin. *Introduction to Hamiltonian Dynamical Systems and the N-body Problem.* Springer, 2008.

[7] W. H. Press, S. A. Teukolsky, W. T. Vetterling, and B. P. Flannery. *Numerical recipes 3rd Edition: The Art of Scientific Computing.* Cambridge University Press, 2007.

[8] Daniel J. Scheeres. *Orbital Motion in Strongly Perturbed Environments: Applications to Asteroid, Comet, and Planetary Satellite Orbiters.* Springer, 2016.